

1
2
3
4
5
6
7
8
9
10
11
12
13
14
15
16
17
18
19
20
21
22
23
24
25

Contact mechanics and lubrication analyses of ceramic-on-metal total hip replacements

Qingen Meng^{a, *}, Feng Liu^a, John Fisher^a, Zhongmin Jin^{a, b}

^a Institute of Medical and Biological Engineering,
School of Mechanical Engineering,
University of Leeds, UK

^b School of Mechanical Engineering,
Xi'an Jiaotong University, China

* Corresponding author

Tel: 44 113 343 5011

Fax: 44 113 242 4611

Email: Q.Meng@leeds.ac.uk

1 **Abstract:**

2

3 Ceramic-on-metal (CoM) total hip replacements have shown reduced wear and
4 friction. Lubrication and contact mechanics analyses play an important role in
5 providing an overall understanding for the tribological performance of CoM bearings.
6 In the present study, the steady-state contact mechanics and elastohydrodynamic
7 lubrication (EHL) and transient EHL of CoM bearings were analysed. The dry and
8 lubricated contact pressures of CoM bearings showed typical characteristics of hard-
9 on-hard hip bearings. The effects of head radius and radial clearance on the
10 lubrication performance were predicted. CoC and CoM bearings are more likely to
11 benefit full fluid film lubrication than MoM bearings.

12

13 **Keywords:** Contact mechanics, Lubrication, Total hip replacement (THR), Ceramic-
14 on-metal (CoM)

15

16

17

18

19

20

21

22

23

24

1 **1. Introduction**

2
3 Metal-on-metal (MoM) bearings made from high-carbon cobalt-chromium (CoCr)
4 alloys have been used for both conventional total hip replacement (THR) and surface
5 replacement in recent years due to reduced volumetric wear and larger bearing size
6 giving improved stability. However, the potential long-term effects of elevated levels
7 of metal ions have remained a concern [1-3] along with the very high failure rates that
8 have been reported for one type of MoM resurfacing implant [4]. A new bearing
9 couple, ceramic-on-metal (CoM), consisting of a ceramic head articulating against a
10 metal acetabular liner, has been shown to reduce wear and friction compared to MoM
11 bearings *in vitro* [5-9]. Moreover, a blood metal ion levels measurement indicated that
12 the chromium levels were significantly lower in CoM than in MoM bearings *in vivo*
13 [10]. Recent studies showed that an increase in the size of ceramic head may reduce
14 wear further [11-13]. Therefore, CoM bearing couple is a promising novel design for
15 hip implants and it has been approved recently by The United States Food and Drug
16 Administration [14].

17
18 Improved lubrication may be an important reason for the lower wear of CoM bearings,
19 since an effective lubricant film between the bearing surfaces can sustain the applied
20 load while avoids direct asperity contacts. The heavy loads and low entrainment
21 velocities experienced by hip implants result in a fluid film pressure distribution that
22 is very close to the dry (unlubricated) contact pressure. Under adverse conditions,
23 such as when the entrainment velocities approach zero and/or the load are very high,
24 lubricant film may break down. Load is consequently sustained by the direct contact
25 of bearing surfaces. Therefore, both dry contact mechanics and lubrication analyses
26 are important for CoM hip bearings. Computational modelling of lubrication and dry

1 contact mechanics of hip replacements can provide detailed information not only for
2 the pressure distribution and lubricant film thickness in contact area, but also for how
3 design and manufacturing parameters and operating conditions affect the lubrication
4 performance. This information is imperative for further insights into the failure of
5 lubricating film, wear generation and design optimization of hip implants, especially
6 for a newly-developed design like CoM hip bearing.

7
8 However, no dry contact mechanics studies have been reported for this promising
9 bearing couple. Moreover, the reported theoretical estimations of the lubrication film
10 of CoM hip bearings were all simply based on a Hamrock-Dowson (H-D) formula [7,
11 15, 16], which can only calculate the minimum film thickness under steady-state
12 conditions. Therefore, the aim of this study was to analyze the contact mechanics and
13 lubrication of CoM hip bearings using numerical methods. The steady-state contact
14 mechanics and elastohydrodynamic lubrication (EHL) and the transient EHL of CoM
15 hip bearings were solved; the effects of geometric parameters of CoM hip bearings on
16 the contact mechanics and lubrication performance were investigated; and the
17 lubrication performances of MoM, CoM and ceramic-on-ceramic (CoC) hip bearings
18 were compared.

19

20 **2. Materials and methods**

21 **2.1 Materials**

22

23 A typical CoM THR bearing normally consists of three components, a titanium
24 acetabular shell, a CoCr insert and a ceramic (typically, alumina or alumina matrix
25 composite) head. The CoCr insert is fixed in the titanium acetabular shell using a
26 taper locking mechanism. The acetabular shell is fixed in the acetabulum using a

1 cementless method. The initial stability of the acetabular shell is achieved by screws
2 or spikes while the long term fixation is reached by the in-growth of bone onto and
3 around the porous-coated shell surface. The spherical ceramic head articulates against
4 the hemi-spherical inner surface of the CoCr insert to form a joint. In the present
5 study, the taper lock between the insert and the shell was not modelled and thus a
6 secure locking between the insert and shell was assumed. A uniform thickness of 10
7 mm and 4 mm was adopted for the CoCr insert and the titanium shell, respectively.
8 The bone and the fixation of the shell were represented by an equivalent support layer
9 with a thickness of 2 mm and appropriate material properties [17]. Such a CoM
10 bearing configuration is shown in Figure 1. All the materials were assumed to be
11 homogeneous and linear elastic. The material properties adopted in the present study
12 are summarized in Table 1. Five CoM THRs with different sizes or radial clearances
13 were analysed in the present study. For the same radial clearance of 60 μm , three
14 commonly used head radii (14 mm, 16 mm and 18 mm) were investigated. For the
15 radius of 18 mm, radial clearances of 30 μm and 100 μm were also simulated. The
16 study assumed correct alignment between the centre of the cup and centre of the head
17 and theoretical alignment of the acetabular cup and head, such that the contact patch
18 on the head did not intersect the rim of the cup.

19
20 In order to compare the lubrication performance of the CoM hip bearing with those of
21 the CoC and MoM bearings, the transient EHL of a CoC THR and a MoM THR, both
22 with the head radius of 18 mm and the radial clearance of 60 μm , were also modelled.
23 The head of the simulated CoC hip bearing was similar to the CoM bearings, while an
24 alumina insert was used for the acetabular component of the CoC bearing. The
25 structure of the acetabular component of the investigated MoM bearing was similar to
26 the CoM bearings. However, the head of the MoM bearing was made of CoCr alloy.

1

2 **2.2 Models**

3

4 Both steady-state and transient conditions were considered for the EHL models. For
5 the dry contact mechanics models, only the loads used in the steady-state EHL models
6 were imposed. The ball-in-socket geometry shown in Figure 1 was used to study the
7 dry contact mechanics and EHL of CoM hip bearings. Since the inclination of the cup
8 has a negligible effect on the EHL of hip implants provided the contact area is within
9 the cup [18], the cup was positioned horizontally instead of anatomically with an
10 angle of 45°. In reality, both the load and velocity experienced in human hip joints are
11 three-dimensional (3D) and time-dependent [19]. Since the major velocity component
12 of hip implants is in the flexion/extension direction and the resultant load is in the
13 direction of about 10° medially to the vertical axis [19], it was possible to
14 approximate the conditions with an estimated small loss in accuracy by considering
15 only the flexion/extension velocity and vertical component of the load. In steady-state
16 EHL studies, the angular velocity around the z axis was adopted as 2 rad/s [17, 20].
17 The vertical load was chosen as 3000 N to represent approximately 4 times normal
18 body weight. In the transient analyses, the walking conditions based on the ISO
19 14242-1 testing standard [21] (Figure 2) were adopted.

20

21 The lubricant in artificial hip joints is periprosthetic synovial fluid, which behaves as
22 a powerful non-Newtonian fluid under relatively low shear rates. However, under
23 higher shear rates likely to be experienced in the hip joint ($10^5/s$), it was considered
24 reasonable to assume the periprosthetic synovial fluid as Newtonian, isoviscous and
25 incompressible [20, 22-24]. A realistic viscosity of 0.002 Pa s was adopted for the
26 synovial fluid in the present study [23].

1
 2 The governing equations for EHL models were established in spherical coordinates
 3 defined in Figure 3. The Reynolds equation for the fluid flow between the bearing
 4 surfaces was

$$5 \quad \sin \theta \frac{\partial}{\partial \theta} \left(h^3 \sin \theta \frac{\partial p}{\partial \theta} \right) + \frac{\partial}{\partial \phi} \left(h^3 \frac{\partial p}{\partial \phi} \right) = 6\eta R_h^2 \sin^2 \theta \left(\omega \frac{\partial h}{\partial \phi} + 2\Gamma \frac{\partial h}{\partial t} \right) \quad (1)$$

6 where p is film pressure; h is film thickness; η is the viscosity of the periprosthetic
 7 synovial fluid; t is time; ω is the angular velocity of femoral head; ϕ and θ are
 8 spherical coordinates defined in Figure 3. The Γ parameter plays the role of a switch,
 9 which could be one or zero to represent a transient or steady-state problem,
 10 respectively.

11
 12 Boundary conditions for the Reynolds equation were

$$13 \quad p(0, \theta) = p(\pi, \theta) = p(\phi, 0) = p(\phi, \pi) = 0$$

$$14 \quad \frac{\partial p}{\partial \phi} = \frac{\partial p}{\partial \theta} = 0 \quad (2)$$

15 The film thickness consisted of the undeformed gap and the elastic deformation of
 16 bearing surfaces due to the film pressure:

$$17 \quad h = c - e_x \sin \theta \cos \phi - e_y \sin \theta \sin \phi + \delta \quad (3)$$

18 where c is the radial clearance between the insert and the head ($c = R_c - R_h$; R_c and R_h
 19 are the radii of the insert and the head, respectively); e_x and e_y are eccentricities of the
 20 femoral head; δ is the elastic deformation of bearing surfaces, determined by the
 21 deformation coefficients of the bearing surfaces and the film pressure.

22
 23 In addition, the external load components were balanced by the integration of the film
 24 pressure:

$$25 \quad f_x = R_h^2 \int_0^\pi \int_0^\pi p \sin^2 \theta \cos \phi \, d\theta \, d\phi = 0$$

$$\begin{aligned}
 f_y &= R_h^2 \int_0^\pi \int_0^\pi p \sin^2 \theta \sin \phi \, d\theta \, d\phi = w_y \\
 f_z &= R_h^2 \int_0^\pi \int_0^\pi p \sin \theta \cos \theta \, d\theta \, d\phi = 0
 \end{aligned}
 \tag{4}$$

2.3 Methods

2.3.1 Dry contact mechanics

3D finite-element (FE) models incorporating the acetabular insert, titanium shell, equivalent support layer and femoral head were created in NX I-DEAS (Version 6.1, Siemens PLM Software Inc., Plano, USA) and solved using ABAQUS (version 6.9-EF1, Dassault Systèmes Simulia Corp., Providence, United States). A mesh convergence study was performed for the bearing with the radius of 18 mm and clearance of 60 μm to determine a proper mesh density. An increase of mesh density from 96×96 elements to 128×128 elements on the contact surface did not generate appreciable differences in the profile of contact pressure distribution. The differences in the maximum pressure and contact area caused by the two mesh densities were only 0.05 percent and 6 percent, respectively. Therefore, the mesh density of 96×96 elements on the contact surface was employed for all the cases, resulting in a total of approximately 129,000 8-node linear brick and 6-node linear triangular prism elements for each dry contact model.

The element-based surfaces of the insert and head were defined as a contact pair, with the insert surface being chosen as the slave surface. “Node to surface” contact discretization was used for the contact pair. “Small sliding” was used as the contact tracking approach. The option of “adjust = 0.0” was adopted to avoid the initial overclosure. The parameter “CLEARANCE”, able to define initial clearance values

1 precisely at slave nodes, was used to accurately specify the initial gap between the
2 bearing surfaces.

3
4 The dry contact mechanics of CoM THR's was also calculated using Hertz contact
5 theory, based on the assumption of semi-infinite solids for the ceramic and metal
6 bearing surfaces. This was done by means of an equivalent ball-on-plane model. The
7 radius of the equivalent ball, R , was determined from the radii of the insert and head,
8 R_c and R_h , and the radial clearance, c :

$$9 \quad R = \frac{R_c R_h}{c} \quad (5)$$

10 This enabled the contact radius, r , and the maximum contact pressure, p_{\max} , to be
11 determined under given load, w :

$$12 \quad r = \left(\frac{3wR}{E'} \right)^{1/3} \quad (6)$$

$$13 \quad p_{\max} = \frac{3w}{2\pi r^2} \quad (7)$$

14 where E' is the equivalent elastic modulus of the ceramic and metal bearing surfaces,
15 determined by the elastic moduli and Poisson's ratios of the CoCr insert and the
16 ceramic head, E_c , ν_c , E_h and ν_h :

$$17 \quad \frac{1}{E'} = \frac{1}{2} \left(\frac{1-\nu_c^2}{E_c} + \frac{1-\nu_h^2}{E_h} \right) \quad (8)$$

18 19 2.3.2. Elastohydrodynamic lubrication

20
21 Found Briefly, for a steady-state problem, the governing equations were non-
22 dimensionalised to facilitate the numerical analysis and improve the stability of the
23 numerical process; the Reynolds equation was solved using a multi-grid method;
24 while the elastic deformation was calculated using a multi-level multi-integration

1 technique [27, 28]. The load balance was satisfied through adjusting the eccentricities
2 of the head according to the calculated load components from the film pressure. Three
3 levels of grid were used in the multilevel solver. On the finest level, 257 nodes were
4 arranged in both the θ and ϕ directions [18, 29]. For the transient models, the walking
5 cycle was divided into 100 time steps (200 time steps made negligible difference in
6 solutions from 100 time steps). At each time step, the numerical procedure was
7 similar to that of a steady-state problem. The simulation of a transient model started
8 with a steady-state solution. The convergent solutions for film thickness, pressure and
9 eccentricities at one time step were used as initial values for the next time step until
10 four walking cycles were finished, when the cyclic convergence had been achieved.

11
12 The deformation coefficients used to calculate the elastic deformation of the bearing
13 surfaces were calculated using a FE-based method [30]. In brief, FE models were
14 created for cups and heads. A unit pressure was applied to an element located at the
15 centre of the articulating surface of the insert or the head. The displacement
16 distribution along a longitudinal line caused by the unit pressure was calculated using
17 ABAQUS. These displacement coefficients were used to curve fit a displacement
18 influence function making use of spherical distance as the independent variable. The
19 coefficients at each node were subsequently calculated using the curve-fitted function.

20

21 **3. Results**

22

23 Figure 4 shows the contour plots of dry contact pressure distribution at the bearing
24 surface for different R_h , with the same radial clearance of 60 μm . The contour plots of
25 dry contact pressure distribution at the bearing surface for different radial clearances,
26 with the same radius of 18 mm are plotted in Figure 5. For all the cases considered in

1 the present study for the dry contact mechanics of CoM bearings, the maximum
 2 contact pressures and contact areas predicted from the FE method and the Hertz
 3 contact theory are listed in Table 2. The contour plots of film pressure predicted by
 4 steady-state EHL for different radii with the same radial clearance are shown in
 5 Figure 6. Figure 7 shows the contour plots of film pressure predicted by steady-state
 6 EHL for different radial clearances with a fixed R_h of 18 mm. In Figure 8, the
 7 minimum film thickness predicted from the present steady-state EHL model of a CoM
 8 THR ($R_h = 18$ mm, $c = 60$ μ m) is compared with that calculated from the H-D formula
 9 [31, 32], which is as follows

$$10 \quad \frac{h_{\min}}{R} = 2.80 \times \left(\frac{\eta u}{E'R} \right)^{0.65} \left(\frac{w}{E'R^2} \right)^{-0.21} \quad (9)$$

11 where u is the effective entraining velocity, calculated from $u = \omega R_h/2$ for the present
 12 problem. Figure 9 shows the effects of radius and radial clearance on the steady-state
 13 film thickness along the central line in the entraining direction. Figure 10 compares
 14 the central and minimum film thicknesses and the maximum pressure between CoM
 15 THRs with different radii but a similar radial clearance, predicted from transient EHL
 16 models. The central and minimum film thicknesses and the maximum pressure
 17 predicted from transient EHL models for CoM THRs with different radial clearances
 18 are compared in Figure 11. Figure 12 compares the central and minimum film
 19 thicknesses and the maximum pressure of CoC, CoM and MoM THRs, predicted from
 20 transient EHL models.

21

22 **4. Discussion**

23

24 The profiles of the dry contact pressure of CoM THRs investigated in the present
 25 study showed typical characteristics of hard-on-hard hip bearings. As shown in

1 Figures 4 and 5, the maximum pressure was at the centre of the contact area; and the
2 pressure distribution closely resembled the Hertz contact distribution. Moreover, for
3 all the cases solved in the present study, the differences in the maximum contact
4 pressures and contact areas predicted by Hertz contact theory and FE methods were
5 less than 7 percent (Table 2). These characteristics are similar to spherical MoM [17]
6 and CoC [33] total hip bearings with thick cups. It should be noted that the backing
7 materials underneath the CoCr insert in the present study and those in the previous
8 studies on hard-on-hard hip bearings were different. In the present study, the materials
9 underneath the insert were titanium shell and equivalent bone. In the MoM study [17],
10 the backing materials were cement and bone, while in the CoC study [33], the
11 material underneath the ceramic inlay was an ultra-high molecular weight
12 polyethylene inlay. However, similar profiles were obtained for the contact pressure
13 of these three types of THRs. Therefore, it can be expected that for all hard-on-hard
14 hip bearings, if the insert (cup) is thick enough, the backing material underneath the
15 inset (cup) and the curvature associated with the ball-in-socket contact have a small
16 effect on the contact mechanics at the bearing surfaces.

17
18 Since film pressure is almost identical to the dry contact pressure over most of the
19 EHL conjunction, especially under a heavy load such as that considered in the steady-
20 state EHL models of the present study, the similarity between the film pressure and
21 the dry contact pressure is consistent with EHL theory and thus provides some support
22 for the solutions of both the dry contact mechanics and steady-state EHL models. It is
23 clear that the profiles and the magnitudes of the film pressures shown in Figures 6 and
24 7 closely resembled those of the corresponding dry contact pressures shown in
25 Figures 4 and 5. For example, the maximum dry contact pressure for the CoM THR

1 with the radius of 14 mm and clearance of 60 μm was 112.6 MPa, while the
2 corresponding maximum film pressure was 112.06 MPa.

3
4 For most of the steady-state cases investigated in Figure 8, the minimum film
5 thicknesses predicted from the present numerical solution agreed well with the H-D
6 formula, since such a thick-cup CoM hip bearing can be approximated as a ‘semi-
7 infinite solid’ model. However, under heavy load and smaller viscosity, differences in
8 the minimum film thicknesses between the present numerical solution and the H-D
9 formula became obvious. Most likely, this is because when the lubricant film is
10 extremely thin, more mesh nodes are needed to capture the minimum film thickness
11 of the steady-state EHL. It is also possible that the Hamrock-Dowson formula intends
12 to produce slightly thicker minimum film thickness, as indicated in a previous study
13 for MoM hip implants [34]. A further investigation has to involve finer meshes.
14 However, currently, the accurate calculation of the deformation coefficients of the
15 bearing surfaces of hip implants for a large number of nodes is still challenging due to
16 the requirement of extremely large computational cost for FE models.

17
18 The FE solutions of dry contact mechanics (Figures 4 and 5) and full numerical
19 analyses of steady-state (Figures 6, 7, and 9) and transient EHL (Figures 10 and 11)
20 indicated that head radius and radial clearance are important parameters for the
21 tribological performance of CoM THRs in terms of reducing dry and lubricated
22 contact pressure. For given bearing materials, dry contact and film pressures are
23 generally determined by load and contact area. For the same load, the larger the
24 contact area, the lower the dry contact and film pressures. Increasing size of hip
25 replacements or/and reducing clearance between the insert and head can increase the
26 contact area between the surfaces. As shown in Figures 4 and 6 and listed in Table 2,

1 for a fixed radial clearance of 60 μm and a load of 3000 N, increasing R_h from 14 to
2 18 mm resulted in a 50 percent increase in contact area. As a result, the maximum dry
3 contact and film pressures decreased from 112.60 to 78.41 MPa and 112.06 to 78.52
4 MPa, respectively. For a fixed R_h of 18 mm and a load of 3000 N, reducing c from
5 100 to 30 μm resulted in an increase in the contact area from 95.23 to 42.23 mm^2 .
6 Correspondingly, the maximum dry contact and film pressures decreased from 110.50
7 to 49.34 MPa and 111.49 to 48.98 MPa (Figures 5 and 7, Table 2), respectively.
8 Moreover, the effects of radius and radial clearance on the film pressure are also
9 clearly shown in transient EHL analyses (Figures 10 c and 11 c).

10
11 EHL analyses indicated that head radius and radial clearance are important parameters
12 to enhance lubricant film thickness of CoM THRs. With a given angular velocity, a
13 larger head radius improves the effective entraining velocity, entraining more
14 lubricant into the contact conjunction, and slightly increases the contact area, all with
15 the overall effect of increasing the lubricant film thickness. Therefore, an increase in
16 the central and minimum film thicknesses is observed in Figures 9 a and 10 for CoM
17 THRs if the radius increased from 14 to 18 mm. For example, the average increases in
18 the central and minimum film thicknesses in one walking cycle obtained from
19 transient EHL analyses were 45 percent and 80 percent. It should be noted that
20 although it has been recognized that the radius of head is one of the key parameters of
21 enhancing lubrication and minimizing wear of hard-on-hard total hip bearings, to the
22 authors' knowledge, no full numerical analyses of the effect of radius on the
23 lubrication performance of hard-on-hard total hip bearings have been published.
24 Therefore, the full numerical solutions presented in Figures 9 a and 10 are also able to
25 provide theoretical supports for other types of hard-on-hard hip bearing.

26

1 A smaller clearance produces a more conforming geometry. Such a conforming
2 geometry reduces the pressure gradient at the inlet, resulting in the reduction in the
3 Poiseuille flow and an increase in the Couette flow. As a result, more lubricant is
4 allowed to flow into the loaded area to improve lubrication [35]. Therefore, a decrease
5 in radial clearance from 100 to 30 μm caused the increase of film thickness (Figures 9
6 b and 11). The average increases in central and minimum film thicknesses in one
7 walking cycle obtained from transient EHL analyses were twofold and threefold,
8 respectively (Figure 11). This conclusion of the effect of the radial clearance on the
9 lubrication performance of CoM hip bearings obtained from the present full numerical
10 analyses was consistent with a previous study for general hard-on-head bearings based
11 on the H-D formula [32].

12
13 The predictions of the effects of radius and radial clearance on the lubrication
14 performance of CoM THRs made in the present study can be validated by published
15 wear test results. Wear and lubrication are closely linked from a tribological point of
16 view. An effective lubricant film is able to reduce wear significantly, while severe
17 wear may occur if the lubricant film is not thick enough to separate the bearing
18 surfaces. It has been shown that with similar or larger average radial clearances, 36-
19 mm-diameter CoM bearings generated significantly lower volumetric loss than 32-
20 mm-diameter CoM bearings [11, 12]. It has also been reported that the wear rate of
21 38-mm-diameter CoM bearings demonstrated lower wear rate than 32-mm-diameter
22 CoM bearings, even though radial clearance of 38-mm-diameter CoM bearings was
23 larger [13]. These results were all consistent with the effect of head radius on the
24 lubrication performance of CoM THRs predicted in the present study. A smaller radial
25 clearance producing increased film thickness agreed well with a simulator wear test of

1 CoM bearings [36], in which small clearances showed low wear than larger clearances
2 for 28-mm-diameter CoM bearings.

3
4 The film thickness of CoM THR was thicker than that of the CoC THR, but thinner
5 than that of the MoM (Figure 12), as expected. Under the same walking conditions,
6 the only factor causing differences in the film thicknesses of the three types of bearing
7 was the material properties of the components, which generated different elastic
8 deformation under the same load. Since the elastic modulus of alumina is larger than
9 that of CoCr alloy, the deformation for hip bearings with ceramic components was
10 smaller, producing a thinner lubricant film. However, it is interesting to estimate the
11 mode of lubrication of the three types of hip prosthesis. The estimation is usually
12 based on the lambda ratio, which can be defined as:

13
$$\lambda = \frac{h_{\min}}{\sqrt{R_{a(\text{head})}^2 + R_{a(\text{cup})}^2}} \quad (10)$$

14 where h_{\min} is the minimum film thickness during a walking cycle; $R_{a(\text{head})}$ and $R_{a(\text{cup})}$
15 are average roughnesses of the head and cup/insert respectively. In the present study, 4
16 nm for ceramic surface roughness and 10 nm for CoCr surface roughness were
17 adopted [7], resulting in composite roughnesses of 5.66, 10.78 and 14.14 nm for CoC,
18 CoM and MoM bearings, respectively. As shown in Figure 12, with similar structure
19 and geometry, the CoC THR may operate in fluid film lubrication during the whole
20 walking gait; the CoM THR benefited fluid film lubrication during 80 percent of a
21 walking cycle; but the MoM THR only operated in fluid film lubrication during 30
22 percent of a walking cycle. Such an improvement of lubrication mode in CoM hip
23 bearing may contribute to the reduction of metallic wear and friction of CoM hip
24 bearings, compared with MoM hip bearings [5-9].

25

1 There are a few limitations in the present study. For example, the roughness of the
2 bearing surfaces, which plays an important role in the lubrication and wear of hip
3 bearings, was not considered in the EHL solution. Moreover, only steady-state and
4 normal walking conditions were considered in the present study. However, under
5 adverse conditions such as start-up and stopping of walking, the lubrication
6 performance and wear of hip bearings could be significantly different from normal
7 walking. It should also be pointed out that the mechanism for the reduced wear of the
8 CoM hip bearings is complicated. Besides the improvement of lubrication, other
9 factors of CoM hip bearings, such as the improvement of hardness, differential
10 hardness reducing adhesive wear [8], and reduction in corrosive wear [37] may also
11 contribute to the lower wear of this novel hip bearing. Furthermore, an enhancement
12 of fluid lubrication may also help in establishment of an effective nano boundary layer
13 on the surface of the metal [38].

14

15 **5. Conclusion**

16

17 For the first time, the dry contact mechanics, steady-state and transient EHL of CoM
18 hip bearings were solved using full numerical methods. Typical dry contact and film
19 pressure distributions and film profiles were predicted for CoM THRs. The effects of
20 the geometric parameters, R_2 and c , on lubricated and unlubricated pressure
21 distributions and steady-state and transient fluid film thicknesses were analyzed. The
22 lubrication performance of CoM hip bearing was compared with that of CoC and
23 MoM hip bearings. The following conclusions can be drawn from this study:

24 (1) The profiles of the dry and lubricated contact pressures of CoM THRs
25 showed typical characteristics of hard-on-hard hip bearings: the maximum

1 pressure was at the centre of the contact area; the pressure distribution
2 closely resembled the Hertz contact distribution.

3 (2) Full numerical analyses of contact mechanics and EHL models indicated
4 that head radius and radial clearance are important parameters in the contact
5 mechanics and EHL of CoM THRs. Increasing head radius and reducing
6 radial clearance reduced contact pressure and enhanced lubricant film.

7 (3) The effects of head radius and radial clearance on lubrication performance
8 were consistent with wear tests of CoM hip bearings reported in the
9 literature.

10 (4) The film thickness of CoM hip bearing was thicker than that of the CoC hip
11 bearing, but thinner than that of the MoM hip bearing. However, CoC and
12 CoM hip bearings are more likely to benefit full fluid film lubrication than
13 MoM hip bearings.

14

15 **6. Acknowledgement**

16

17 This work was supported by EPSRC and partly supported by the NIHR (National
18 Institute for Health Research) as part of collaboration with the LMBRU (Leeds
19 Musculoskeletal Biomedical Research Unit). JF is an NIHR Senior Fellow.

20

21

22 **Conflict of interest statement**

23

24 JF is a consultant to DePuy, the manufacturer of CoM MoM and CoC bearings. The
25 University of Leeds and JF receive royalty income from DePuy arising from the
26 transfer of intellectual property on bearing technology.

- 1
- 2
- 3
- 4
- 5
- 6
- 7
- 8
- 9
- 10
- 11
- 12
- 13
- 14
- 15
- 16
- 17
- 18
- 19
- 20
- 21

References:

1. Brown C, Fisher J, Ingham E. Biological effects of clinically relevant wear particles from metal-on-metal hip prostheses. *Proceedings of the Institution of Mechanical Engineers, Part H: Journal of Engineering in Medicine* 2006; 220(H2): 355-369.
2. Crawford R, Ranawat CS, Rothman RH. Metal on Metal: Is It Worth the Risk? *Journal of Arthroplasty* 2010; 25(1): 1-2.
3. Haddad FS, Thakrar RR, Hart AJ, Skinner JA, Nargol AVF, Nolan JF, et al. Metal-on-metal bearings THE EVIDENCE SO FAR. *Journal of Bone and Joint Surgery-British Volume* 2011; 93B(5): 572-579.
4. Langton DJ, Joyce TJ, Jameson SS, Lord J, Van Orsouw M, Holland JP, et al. Adverse reaction to metal debris following hip resurfacing - The influence of component type, orientation and volumetric wear. *Journal of Bone and Joint Surgery-British Volume* 2011; 93B(2): 164-171.
5. Firkins PJ, Tipper JL, Ingham E, Stone MH, Farrar R, Fisher J. A novel low wearing differential hardness, ceramic-on-metal hip joint prosthesis. *Journal of Biomechanics* 2001; 34(10): 1291-1298.
6. Williams S, Schepers A, Isaac G, Hardaker C, Ingham E, van der Jagt D, et al. The 2007 Otto Aufranc Award. Ceramic-on-metal hip arthroplasties: a comparative in vitro and in vivo study. *Clinical Orthopaedics and Related Research* 2007; 465: 23-32.
7. Brockett C, Williams S, Jin ZM, Isaac G, Fisher J. Friction of total hip replacements with different bearings and loading conditions. *Journal of Biomedical Materials Research Part B-Applied Biomaterials* 2007; 81B(2): 508-515.
8. Barnes CL, DeBoer D, Corpe RS, Nambu S, Carroll M, Timmerman I. Wear performance of large-diameter differential-hardness hip bearings. *Journal of Arthroplasty* 2008; 23(6): 56-60.
9. Bishop NE, Waldow F, Morlock MM. Friction moments of large metal-on-metal hip joint bearings and other modern designs. *Medical Engineering & Physics* 2008; 30(8): 1057-1064.
10. Isaac GH, Brockett C, Breckon A, van der Jagt D, Williams S, Hardaker C, et al. Ceramic-on-metal bearings in total hip replacement - Whole blood metal ion levels and analysis of retrieved components. *Journal of Bone and Joint Surgery-British Volume* 2009; 91B(9): 1134-1141.
11. Affatato S, Spinelli M, Squarzone S, Traina F, Toni A. Mixing and matching in ceramic-on-metal hip arthroplasty: An in-vitro hip simulator study. *Journal of*

- Biomechanics 2009; 42(15): 2439-2446.
12. Affatato S, Spinelli M, Zavalloni M, Traina F, Carmignato S, Toni A. Ceramic-On-Metal for Total Hip Replacement: Mixing and Matching Can Lead to High Wear. *Artificial Organs* 2010; 34(4): 319-323.
 13. Ishida T, Clarke IC, Donaldson TK, Shirasu H, Shishido T, Yamamoto K. Comparing Ceramic-Metal to Metal-Metal Total Hip Replacements-A Simulator Study of Metal Wear and Ion Release in 32-and 38-mm Bearings. *Journal of Biomedical Materials Research Part B-Applied Biomaterials* 2009; 91B(2): 887-896.
 14. FDA approves first ceramic-on-metal total hip replacement system. [updated 06/14/2011 cited 10/16/2011]; Available from: <http://www.fda.gov/NewsEvents/Newsroom/PressAnnouncements/ucm259061.htm>.
 15. Dowson D. New joints for the Millennium: wear control in total replacement hip joints. *Proceedings of the Institution of Mechanical Engineers Part H-Journal of Engineering in Medicine* 2001; 215(H4): 335-358.
 16. Williams SR, Wu JJ, Unsworth A, Khan I. Tribological and surface analysis of 38 mm alumina-as-cast Co-Cr-Mo total hip arthroplasties. *Proceedings of the Institution of Mechanical Engineers Part H-Journal of Engineering in Medicine* 2009; 223(H8): 941-954.
 17. Jagatia M, Jin ZM. Elastohydrodynamic lubrication analysis of metal-on-metal hip prostheses under steady state entraining motion. *Proceedings of the Institution of Mechanical Engineers Part H-Journal of Engineering in Medicine* 2001; 215(H6): 531-541.
 18. Wang FC, Jin ZM. Transient elastohydrodynamic lubrication of hip joint implants. *Journal of Tribology-Transactions of the ASME* 2008; 130(1): 011007.
 19. Bergmann G, Deuretzbacher G, Heller M, Graichen F, Rohlmann A, Strauss J, et al. Hip contact forces and gait patterns from routine activities. *Journal of Biomechanics* 2001; 34(7): 859-871.
 20. Jin ZM. Theoretical studies of elastohydrodynamic lubrication of artificial hip joints. *Proceedings of the Institution of Mechanical Engineers, Part J: Journal of Engineering Tribology* 2006; 220(J8): 719-727.
 21. ISO 14242-1, Implants for Surgery - Wear of Total Hip-Joint Prostheses - Part 1: Loading and Displacement Parameters for Wear-Testing Machines and Corresponding Environmental Conditions for Test. 2002.
 22. Cooke AF, Dowson D, Wright V. The rheology of synovial fluid and some potential synthetic lubricants for degenerate synovial joints. *Engineering in Medicine* 1978; 7: 66-72.

23. Yao JQ, Laurent MP, Johnson TS, Blanchard CR, Crowninshield RD. The influences of lubricant and material on polymer/CoCr sliding friction. *Wear* 2003; 255(1-6): 780-784.
24. Wang WZ, Jin ZM, Dowson D, Hu YZ. A study of the effect of model geometry and lubricant rheology upon the elastohydrodynamic lubrication performance of metal-on-metal hip joints. *Proceedings of the Institution of Mechanical Engineers Part J-Journal of Engineering Tribology* 2008; 222(J3): 493-501.
25. Meng QE, Gao LM, Liu F, Yang PR, Fisher J, Jin ZM. Transient elastohydrodynamic lubrication analysis of a novel metal-on-metal hip prosthesis with an aspherical acetabular bearing surface. *Journal of Medical Biomechanics* 2009; 24(5): 352-362.
26. Gao L, Wang F, Yang P, Jin Z. Effect of 3D physiological loading and motion on elastohydrodynamic lubrication of metal-on-metal total hip replacements. *Medical Engineering & Physics* 2009; 31(6): 720-729.
27. Gao LM, Meng QE, Wang FC, Yang PR, Jin ZM. Comparison of numerical methods for elastohydrodynamic lubrication analysis of metal-on-metal hip implants: multi-grid verses Newton-Raphson. *Proceedings of the Institution of Mechanical Engineers, Part J: Journal of Engineering Tribology* 2007; 221(J2): 133-140.
28. Venner CH, Multigrid solution of the EHL line and point contact problems. PhD Thesis. 1991, Enschede: University of Twente.
29. Liu F, Jin ZM, Hirt F, Rieker C, Roberts P, Grigoris P. Transient elastohydrodynamic lubrication analysis of metal-on-metal hip implant under simulated walking conditions. *Journal of Biomechanics* 2006 a; 39(5): 905-914.
30. Wang FC, Jin ZM. Prediction of elastic deformation of acetabular cups and femoral heads for lubrication analysis of artificial hip joints. *Proceedings of the Institution of Mechanical Engineers Part J-Journal of Engineering Tribology* 2004 a; 218(J3): 201-209.
31. Hamrock BJ, Dowson D. Elastohydrodynamic lubrication of elliptical contacts for materials of low elastic-modulus. I: Fully flooded conjunction. *Journal of Lubrication Technology-Transactions of the ASME* 1978; 100(2): 236-245.
32. Jin ZM, Dowson D, Fisher J. Analysis of fluid film lubrication in artificial hip joint replacements with surfaces of high elastic modulus. *Proceedings of the Institution of Mechanical Engineers Part H-Journal of Engineering in Medicine* 1997; 211(3): 247-256.
33. Mak MM, Jin ZM. Analysis of contact mechanics in ceramic-on-ceramic hip joint replacements. *Proceedings of the Institution of Mechanical Engineers*

Part H-Journal of Engineering in Medicine 2002; 216(H4): 231-236.

34. Jalali-Vahid D, Jin ZM, Dowson D. Isoviscous elastohydrodynamic lubrication of circular point contacts with particular reference to metal-on-metal hip implants. Proceedings of the Institution of Mechanical Engineers Part J-Journal of Engineering Tribology 2003; 217(J5): 397-402.
35. Meng QE, Liu F, Fisher J, Jin ZM. Transient elastohydrodynamic lubrication analysis of a novel metal-on-metal hip prosthesis with a non-spherical femoral bearing surface. Proceedings of the Institution of Mechanical Engineers Part H-Journal of Engineering in Medicine 2011; 225(H1): 25-37.
36. Haider H, Weisenburger JN, Naylor MG, Schroeder DW, Croson RE, Garvin KL. Bearing diameter, radial clearance and their effect on wear in ceramic-on-metal total hip replacements. In 54th Annual Meeting of the Orthopaedic Research Society. 2008. San Francisco, California, USA. Poster 1792.
37. Figueiredo-Pina CG, Yan Y, Neville A, Fisher J. Understanding the differences between the wear of metal-on-metal and ceramic-on-metal total hip replacements. Proceedings of the Institution of Mechanical Engineers Part H-Journal of Engineering in Medicine 2008; 222(H3): 285-296.
38. Pourzal R, Theissmann R, Williams S, Gleising B, Fisher J, Fischer A. Subsurface changes of a MoM hip implant below different contact zones. Journal of the Mechanical Behavior of Biomedical Materials 2009; 2(2): 186-191.

Nomenclature:

c	radial clearance between head and insert
e_x, e_y	eccentricity components of the femoral head in x and y directions
E_c, E_h	elastic moduli of insert and head, respectively
E'	equivalent elastic modulus of bearing surfaces
f_x, f_y, f_z	calculated load components
h	film thickness
h_{\min}	the minimum film thickness
p	pressure
r	contact radius calculated from Hertz contact theory
R	radius of the equivalent ball of the equivalent ball-on-plane model
$R_{a(\text{cup})}$	average roughness of the insert
$R_{a(\text{head})}$	average roughness of the head
R_h	radius of femoral head
R_c	radius of the cup/insert
t	time (s)
u	effective entraining velocity
w_y	applied load in y direction
x, y, z	Cartesian coordinates
δ	elastic deformation the femoral head and acetabular cup
η	viscosity of synovial fluid
ϕ, θ	angular coordinates in the entraining and side-leakage directions respectively.
λ	lambda ratio
ν_c, ν_h	Poisson's ratios of insert and head, respectively
ω	angular velocity

Captions

- Table 1 Material properties used for CoCr alloy, titanium, alumina and equivalent support layer
- Table 2 Comparison of the predicted maximum contact pressure and contact area between the present finite element study and the Hertz contact theory
- Figure 1 A ball-in-socket configuration for contact mechanics and EHL analyses of CoM bearings
- Figure 2 Variation in the load (a) and velocity (b) of the walking conditions based on ISO 14242-1
- Figure 3 Definition of spherical coordinates and mesh grid
- Figure 4 Contour plots of dry contact pressure (MPa) at the bearing surface of CoM hip replacements with a similar radial clearance (60 μm) but different radii: (a) 14 mm, (b) 16 mm, (c) 18 mm
- Figure 5 Contour plots of dry contact pressure (MPa) at the bearing surface of CoM hip replacements with a similar radius (18 mm) but different radial clearances: (a) 100 μm , (b) 30 μm
- Figure 6 Contour plots of steady-state film pressure (MPa) in CoM hip replacements with similar radial clearance (60 μm) but different radii: (a) 14 mm, (b) 16 mm, (c) 18 mm
- Figure 7 Contour plots of steady-state film pressure (MPa) in CoM hip replacements with similar radius (18 mm) but different radial clearances: (a) 100 μm , (b) 30 μm
- Figure 8 Minimum film thicknesses produced by the H-D formula and current numerical model for a 36-mm-diameter CoM THR with radial clearance of 60 μm under different loads
- Figure 9 Comparison of steady-state film thickness on the central line along the entraining direction for different radii ($c = 60 \mu\text{m}$) (a) and radial clearances ($R_h = 18 \text{ mm}$) (b)
- Figure 10 Prediction of the central film thickness (a), minimum film thickness (b) and maximum pressure (c) by transient EHL solution for CoM hip replacements with a similar radial clearance (60 μm) but different radii, under transient conditions based on ISO 14242-1

Figure 11 Prediction of the central film thickness (a), minimum film thickness (b) and maximum pressure (c) by transient EHL solution for CoM hip replacements with a similar size (18 mm) but different radial clearances, under transient conditions based on ISO 14242-1

Figure 12 Under transient conditions based on ISO 14242-1, prediction of the central film thickness (a), minimum film thickness (b) and maximum pressure (c) by transient EHL solution for CoM, CoC and MoM hip replacements with similar size (18 mm) and radial clearance (60 μm)

Table 1 Material properties used for CoCr alloy, titanium, alumina and equivalent support layer

	Elastic modulus (GPa)	Poisson's ratio
CoCr	210	0.3
Titanium	110	0.3
Equivalent support layer	2.27	0.23
Alumina	380	0.26

Table 2 Comparison of the predicted maximum contact pressure and contact area between the present finite element study and the Hertz contact theory

Radius (mm)	Radial clearance (μm)	Maximum contact pressure			
		(MPa)		Contact area (mm^2)	
		Finite element	Hertz	Finite element	Hertz
14	60	112.60	105.40	40.51	42.69
16	60	92.89	88.24	48.52	50.99
18	60	78.41	75.44	61.35	59.65
18	30	49.34	47.58	95.29	94.58
18	100	110.50	105.89	42.23	42.50

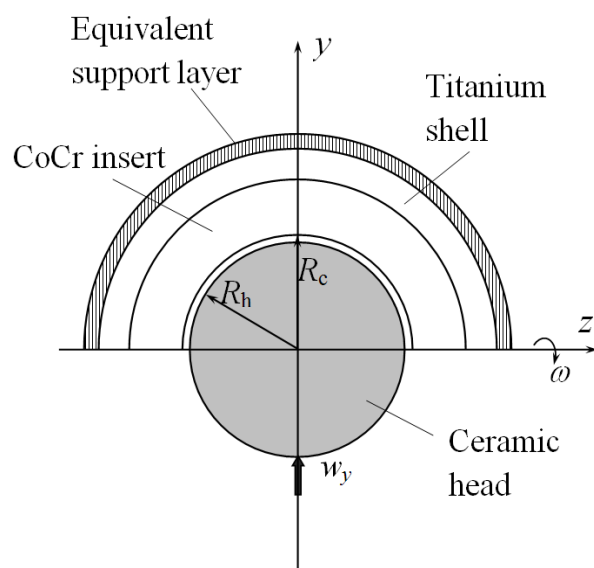


Figure 1 A ball-in-socket configuration for contact mechanics and EHL analyses of CoM bearings

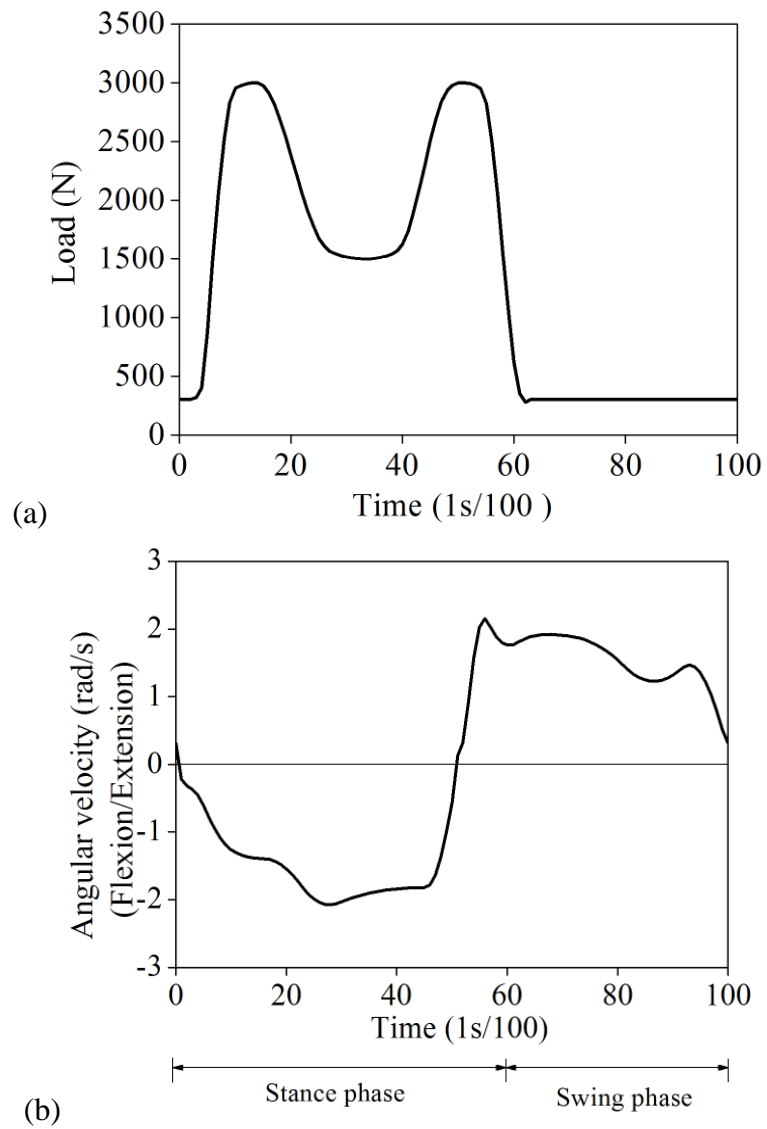


Figure 2 Variation in the load (a) and velocity (b) of the walking conditions based on ISO 14242-1

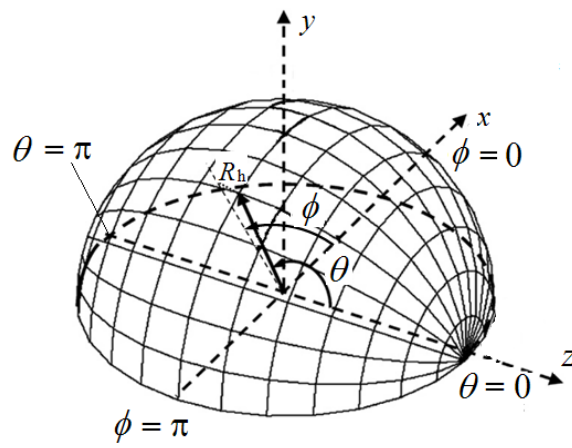


Figure 3 Definition of spherical coordinates and spherical mesh grid

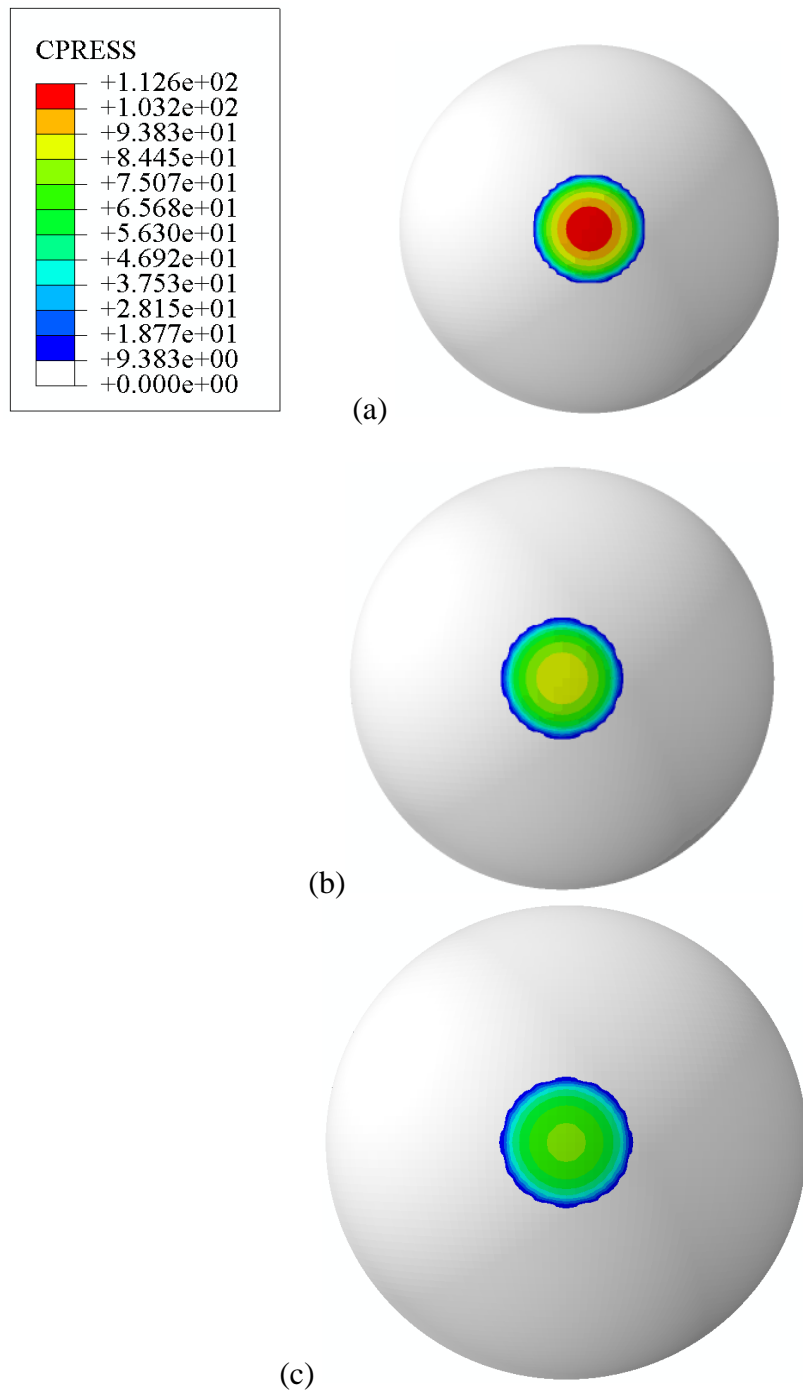


Figure 4 Contour plots of dry contact pressure (MPa) at the bearing surface of CoM hip replacements with a similar radial clearance (60 μm) but different radii: (a) 14 mm, (b) 16 mm, (c) 18 mm

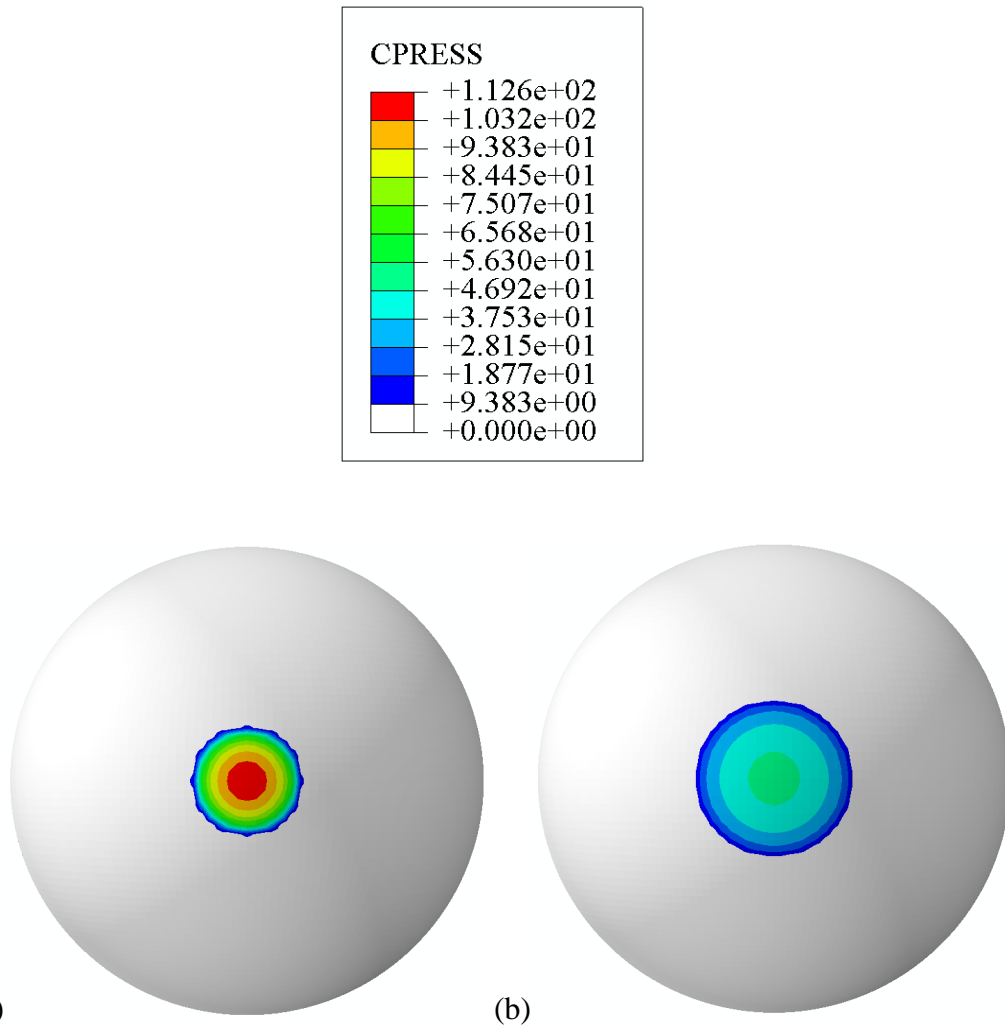


Figure 5 Contour plots of dry contact pressure (MPa) at the bearing surface of CoM hip replacements with a similar radius (18 mm) but different radial clearances: (a) 100 μm , (b) 30 μm

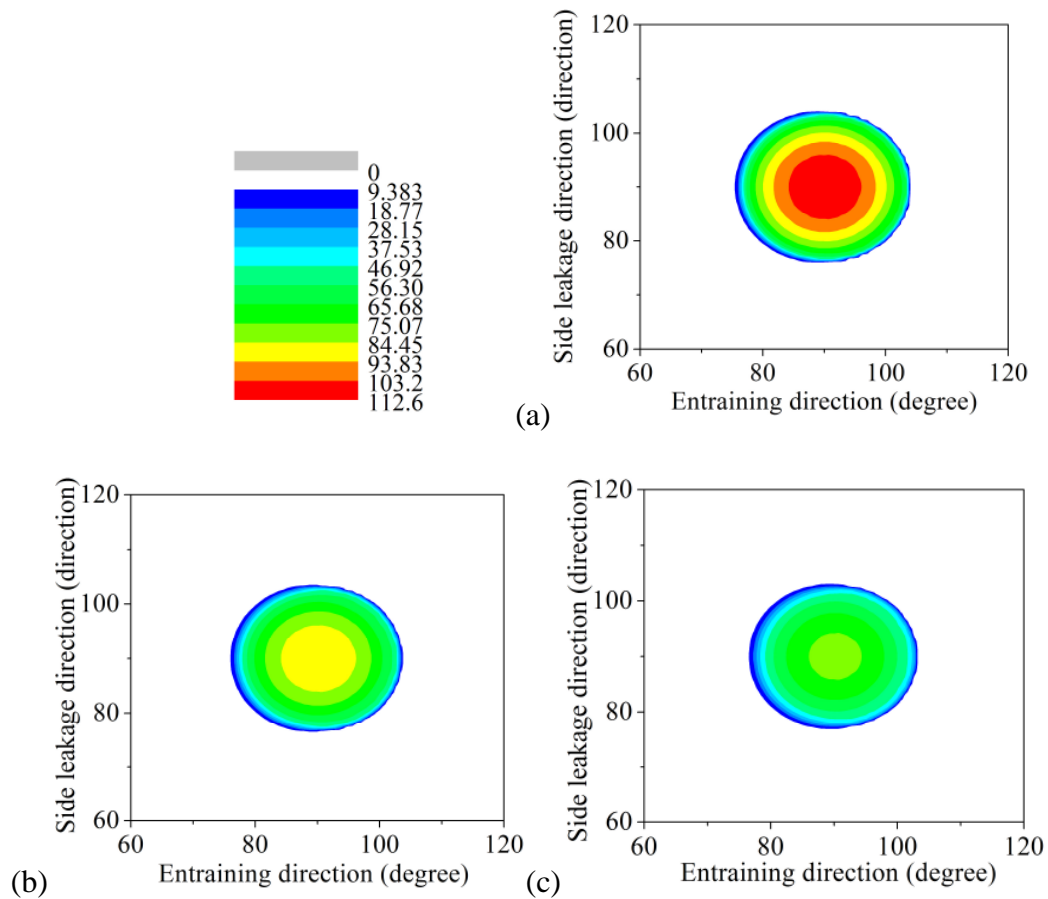


Figure 6 Contour plots of steady-state film pressure (MPa) in CoM hip replacements with similar radial clearance ($60 \mu\text{m}$) but different radii: (a) 14 mm, (b) 16 mm, (c) 18 mm

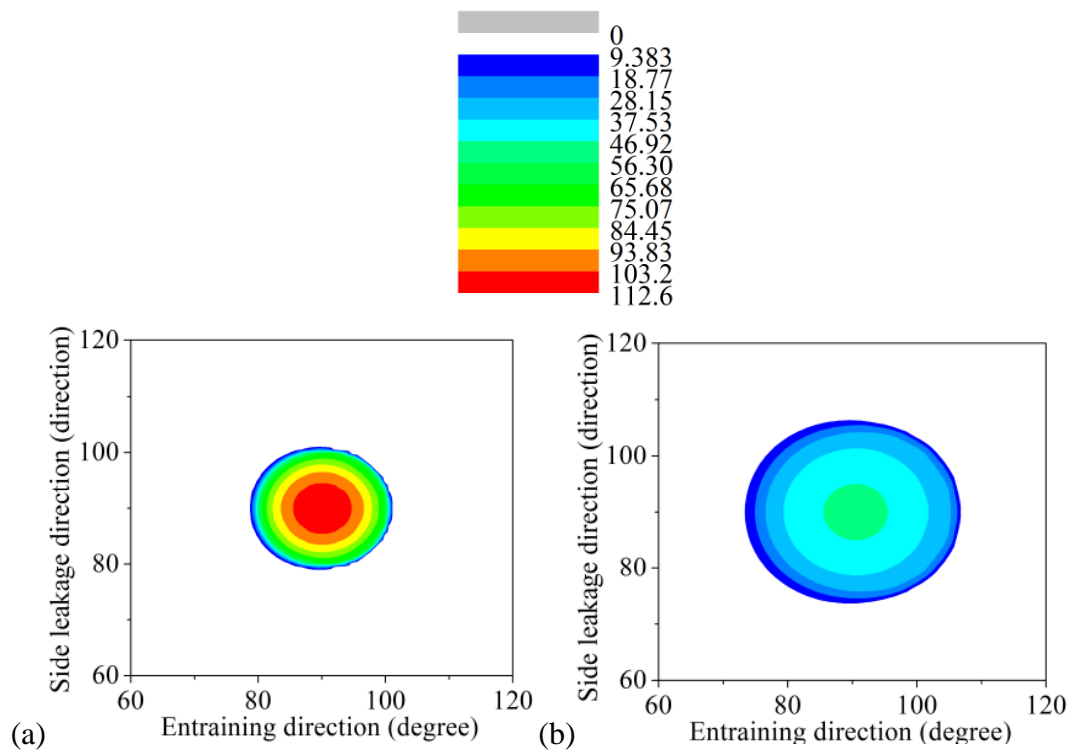


Figure 7 Contour plots of steady-state film pressure (MPa) in CoM hip replacements with similar radius (18 mm) but different radial clearances: (a) 100 μm , (b) 30 μm

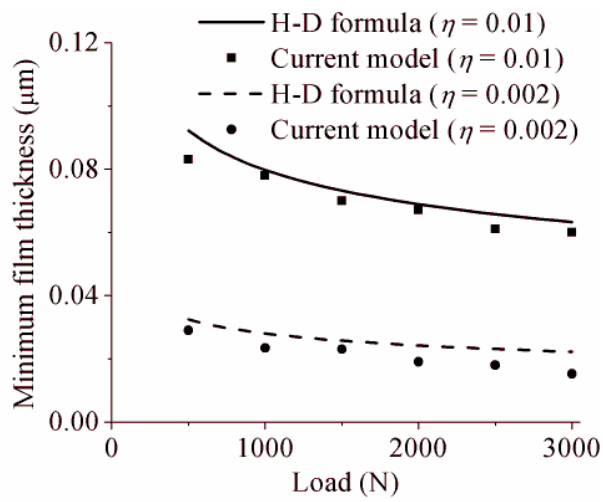


Figure 8 Minimum film thicknesses produced by the H-D formula and current numerical model under different loads for a 36-mm-diameter CoM THR with radial clearance of 60 μm

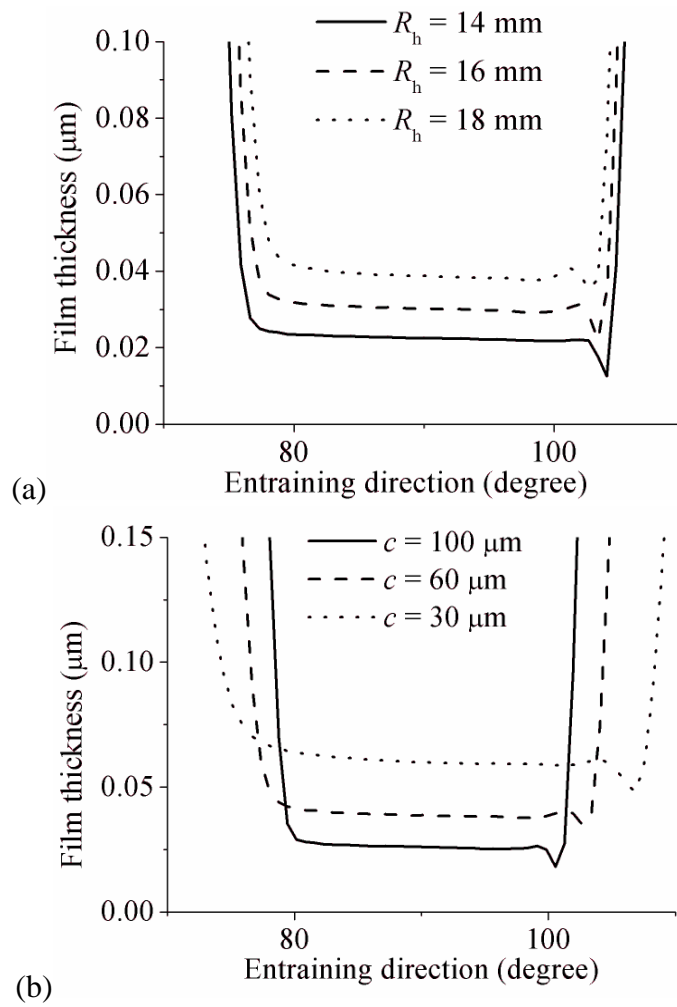


Figure 9 Comparison of steady-state film thickness on the central line along the entraining direction for different radii ($c = 60 \mu\text{m}$) (a) and radial clearances ($R_h = 18 \text{ mm}$) (b)

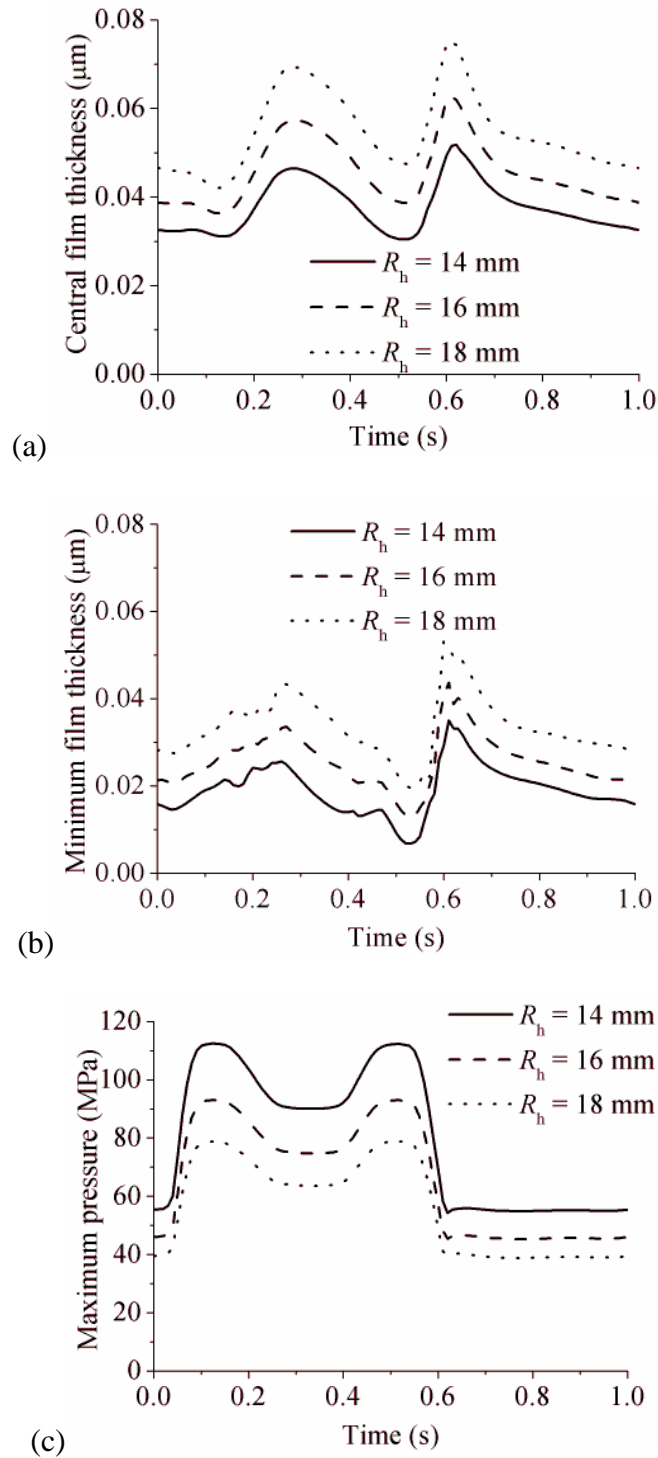


Figure 10 Prediction of the central film thickness (a), minimum film thickness (b) and maximum pressure (c) by transient EHL solution for CoM hip replacements with a similar radial clearance ($60 \mu\text{m}$) but different radii, under transient conditions based on ISO 14242-1

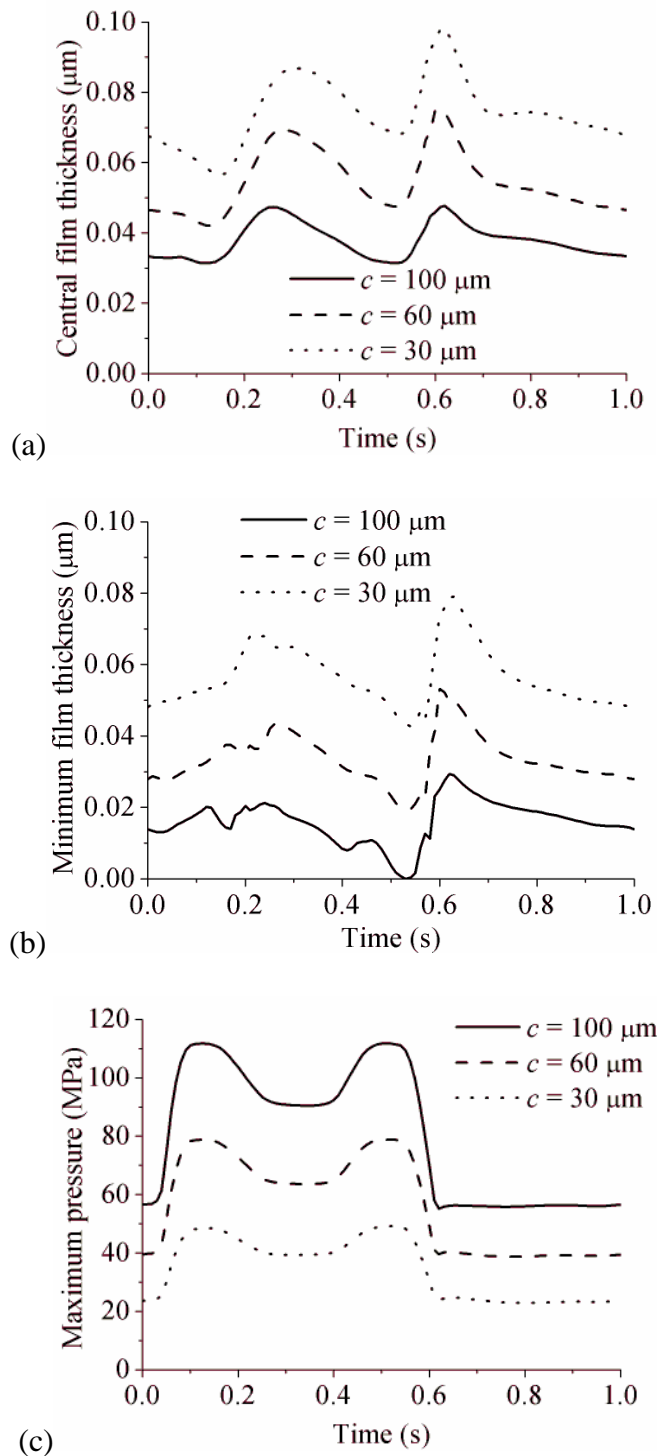


Figure 11 Prediction of the central film thickness (a), minimum film thickness (b) and maximum pressure (c) by transient EHL solution for CoM hip replacements with a similar size (18 mm) but different radial clearances, under transient conditions based on ISO 14242-1

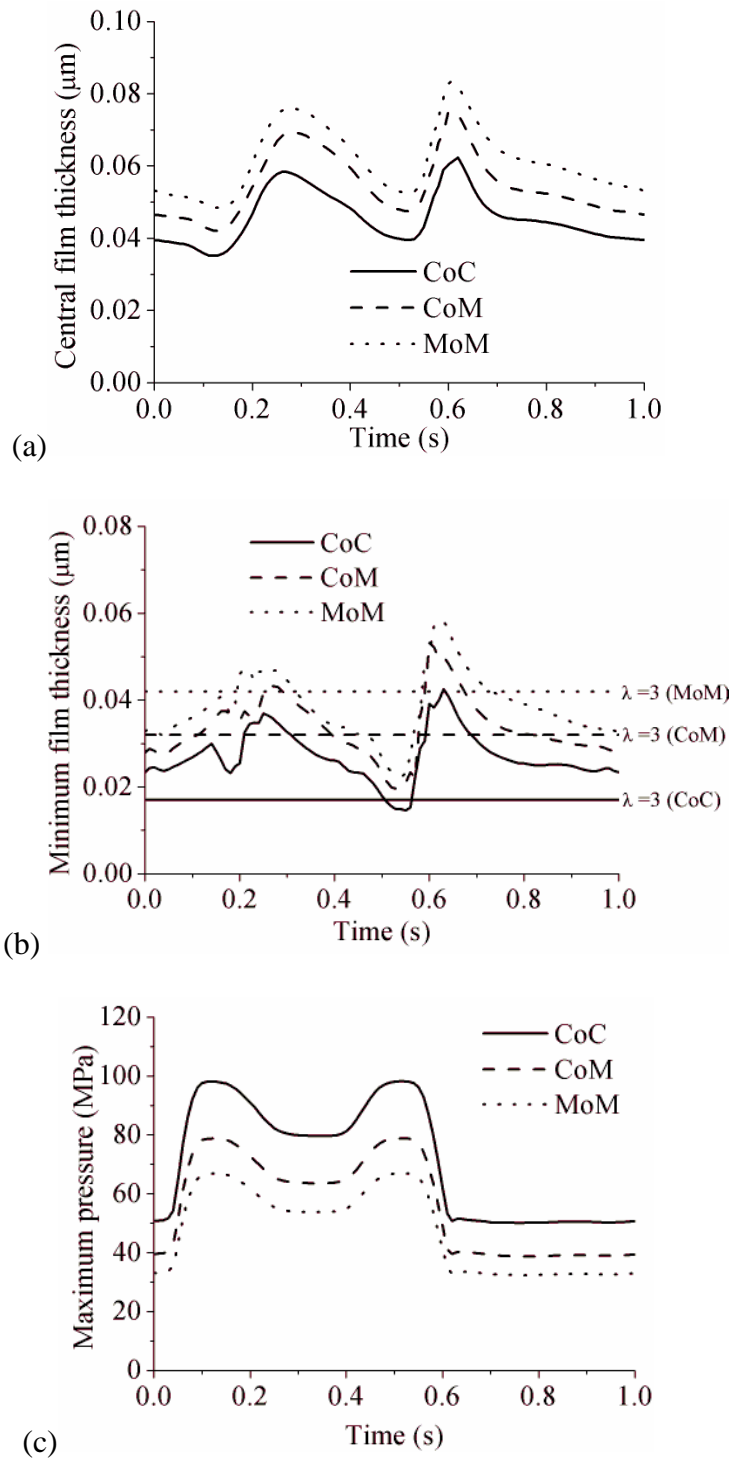


Figure 12 Under transient conditions based on ISO 14242-1, prediction of the central film thickness (a), minimum film thickness (b) and maximum pressure (c) by transient EHL solution for CoM, CoC and MoM hip replacements with similar size (18 mm) and radial clearance (60 μm)